

# THE RECENT AND CONTINUING ASSEMBLY OF FIELD ELLIPTICALS BY RED MERGERS

PIETER G. VAN DOKKUM

Department of Astronomy, Yale University, New Haven, CT 06520-8101; dokkum@astro.yale.edu

*Submitted to the Astronomical Journal, 15 April 2005*

## ABSTRACT

We present a study of tidal debris associated with 126 nearby red galaxies, selected from the 1.2 degree<sup>2</sup> Multiwavelength Survey by Yale-Chile (MUSYC) and the 9.3 degree<sup>2</sup> NOAO Deep Wide-Field Survey. In the full sample 67 galaxies (53 %) show morphological signatures of tidal interactions, consisting of broad fans of stars, tails, and other asymmetries at very faint surface brightness levels. When restricting the sample to the 86 bulge-dominated early-type galaxies the fraction of tidally disturbed galaxies rises to 71 %, which implies that for every “normal” undisturbed elliptical there are two which show clear signs of interactions. The tidal features are red and smooth, and often extend over  $> 50$  kpc. Of the tidally distorted galaxies about 2/3 are remnants and 1/3 are interacting with a companion galaxy. The companions are usually bright red galaxies as well: the median  $R$ -band luminosity ratio of the tidal pairs is 0.31, and the median color difference after correcting for the slope of the color-magnitude relation is  $-0.02$  in  $B - R$ . If the ongoing mergers are representative for the progenitors of the remnants  $\sim 35$  % of bulge-dominated galaxies experienced a merger with mass ratio  $> 1 : 4$  in the recent past. With further assumptions it is estimated that the present-day mass accretion rate of galaxies on the red sequence  $\Delta M/M = 0.09 \pm 0.04 \text{ Gyr}^{-1}$ . For a constant or increasing mass accretion rate with redshift, we find that red mergers may lead to an evolution of a factor of  $\gtrsim 2$  in the stellar mass density in luminous red galaxies over the redshift range  $0 < z < 1$ , consistent with recent studies of the evolution of the luminosity density. We conclude that most of today’s field elliptical galaxies were assembled at low redshift through mergers of gas-poor, bulge-dominated systems. These “dry” mergers are consistent with the high central densities of ellipticals, their old stellar populations, and the strong correlations of their properties. It will be interesting to determine whether this mode of merging only plays an important role at low redshift or is relevant for galaxies at any redshift if they exceed a critical mass scale.

*Subject headings:* galaxies: evolution — galaxies: formation — galaxies: elliptical and lenticular, cD

## 1. INTRODUCTION

Although greatly outnumbered by spiral galaxies, elliptical galaxies contain  $\sim 20$  % of the stellar mass in the present-day Universe (Fukugita, Hogan, & Peebles 1998) and dominate the high mass end of the galaxy mass function (e.g., Nakamura et al. 2003). Their status at the top of the food chain is a strong motivation for their study as it provides insight in the processes governing the build-up of galaxies over cosmic time, the nature of the most luminous galaxies at  $z \sim 3$  and beyond, the formation of the first stars, and the origins of supermassive black holes.

Despite vigorous research efforts it is still not known how and when elliptical galaxies were formed. Separating the time of the formation of their *stars* from the time of their *assembly*, a partial answer is that most of the stars in the most massive ellipticals were formed at high redshift. This result is supported by a large number of studies of nearby and distant galaxies, and applies to ellipticals in the general field as well as those in rich clusters (e.g., Bower, Lucey, & Ellis 1992; Ellis et al. 1997; Bernardi et al. 1998, 2003; van Dokkum et al. 1998a, 1998b; Treu et al. 1999, 2002; van Dokkum et al. 2001a; Holden et al. 2005). Even when accounting for possible selection effects due to morphological evolution (“progenitor bias”; van Dokkum & Franx 2001), it is very difficult to fit the observed evolution of massive ellipticals with formation redshifts substantially lower than  $z \sim 2$ . Although there is general agreement that the mean age is high, there are strong indications that not all stars in all elliptical galaxies formed at high redshift: Trager et al. (2000) and others (e.g., Yi et al. 2005) find evidence for a “sprinkling” of recent star formation in otherwise old ellipticals, and

recent studies of the evolution of the Fundamental Plane relation (Djorgovski & Davis 1987) find evidence that low mass early-type galaxies have lower luminosity-weighted ages than high mass ones (Treu et al. 2005; van der Wel et al. 2005).

Much less is known about the assembly of elliptical galaxies, that is, when and how the galaxies were “put together”. In the literature, a distinction is often made between models in which elliptical galaxies form from the collapse of primordial gas clouds (“monolithic collapse”; e.g., Eggen, Lynden-Bell, & Sandage 1962; Jimenez et al. 1999), or in mergers of smaller galaxies (“hierarchically”; e.g. Toomre & Toomre 1972; White & Frenk 1991). Within the framework of a merger model the question of assembly can be specified as, first, the typical age of the last major merger; and second, the nature of the progenitor galaxies. In many individual cases we can readily answer both questions: abundant evidence leaves little doubt that some ellipticals formed recently through the merger of spiral galaxies, or will do so in the near future (e.g., Toomre & Toomre 1972; Schweizer 1982; Hibbard & van Gorkom 1996). However, it is not clear whether such mergers are exceptional or responsible for the formation of the majority of ellipticals.

Among the observational arguments *for* recent mergers are the detection of “fine-structure” (e.g., shells and ripples) in a large number of nearby ellipticals (Malin & Carter 1983; Schweizer et al. 1990); the presence of kinematically-decoupled cores (Franx & Illingworth 1988; Bender 1988); small-scale dust seen in the majority of ellipticals (e.g., van Dokkum & Franx 1995); (some) studies of the redshift evolution of galaxy morphologies, and of close pairs (e.g., Le Fèvre et al. 2000; Patton et al. 2002; Conselice et al. 2003); and strong evolution of the mass density of red galaxies to  $z \sim 1$ , in-

ferred from the COMBO-17 survey (Bell et al. 2004). Furthermore, and perhaps most importantly, the hierarchical assembly of galaxies is a central aspect of current models for galaxy formation in  $\Lambda$ CDM cosmologies (e.g., Kauffmann, White, & Guiderdoni 1993; Cole et al. 2000; Meza et al. 2003).

Among arguments *against* the merger hypothesis are the low probability of mergers in virialized clusters, which are dominated by ellipticals (Ostriker 1980; Makino & Hut 1997); the fact that the central densities of ellipticals are too high to be the result of dissipationless mergers of pure disks (Carlberg 1986; Hernquist 1992); the low scatter in the color-magnitude relation and Fundamental Plane, which is inconsistent with the diversity in stellar populations expected from spiral galaxy mergers (e.g., Bower, Kodama, & Terlevich 1998, Peebles 2002); the much higher specific frequency of globular clusters for ellipticals than for spirals (although some globulars may be formed during mergers; e.g., Schweizer et al. 1996); the observation that known remnants of spiral galaxy mergers have underluminous X-ray halos (Sansom, Hibbard, & Schweizer 2000); the existence of the  $M_\bullet - \sigma$  relation (Gebhardt et al. 2000; Ferrarese & Merritt 2000); and the presence of massive galaxies at high redshift (e.g., Franx et al. 2003; Daddi et al. 2004; Glazebrook et al. 2004).

These apparently contradictory lines of evidence may be largely reconciled by postulating that most elliptical galaxies formed through (nearly) dissipationless (or “dry”) mergers of red, bulge-dominated galaxies rather than mergers of spiral disks. Motivated by the comparatively red colors of ellipticals exhibiting fine-structure Schweizer & Seitzer (1992) discuss this possibility, but argue that mergers between early-type galaxies are statistically unlikely as the “median” field galaxy is an Sb spiral. However, most mergers likely occur in groups, where the early-type galaxy fraction is much higher than in the general field (e.g., Zabludoff & Mulchaey 1998). Furthermore, semianalytical models of galaxy formation have predicted that the most recent mergers of bright ellipticals were between gas-poor, bulge-dominated galaxies (Kauffmann & Haehnelt 2000; Khochfar & Burkert 2003), and several studies have shown

that such merging is consistent with the observed Fundamental Plane relation (e.g., González-García & van Albada 2003; Boylan-Kolchin, Ma, & Quataert 2005). Finally, mergers between red galaxies may be common in young, unvirialized galaxy clusters at  $z \sim 1$  (van Dokkum et al. 1999, 2001b, Tran et al. 2005).

Although some early-type/early-type mergers are known to exist in the local universe (e.g., Davoust & Prugniel 1988; Combes et al. 1995), little is known about their frequency. Here we investigate the relevance of dry merging by analyzing the frequency and nature of tidal distortions associated with a well-defined sample of bright red galaxies. This study was motivated by the results of Kauffmann & Haehnelt (2000), Khochfar & Burkert (2003), and Bell et al. (2004), the observations of red mergers in  $z \sim 1$  clusters, and the advent of very deep photometric surveys over wide areas. We assume  $\Omega_m = 0.3$ ,  $\Omega_\Lambda = 0.7$ , and  $H_0 = 70 \text{ km s}^{-1} \text{ Mpc}^{-1}$  (Spergel et al. 2003).

## 2. MORPHOLOGICAL SIGNATURES

Mergers between gas-poor, bulge-dominated galaxies are generally more difficult to recognize than mergers between gas-rich disks. Elliptical-elliptical mergers do not develop prominent tidal tails dotted with star forming regions, but are instead characterized by the ejection of broad “fans” of stars, and in certain cases an asymmetric deformation of the inner isophotes (e.g., Rix & White 1989; Balcells & Quinn 1990; Combes et al. 1995). Tails may develop if one of the progenitors rotates or has a disk component (Combes et al. 1995), but as there is no cold, young component these are expected to be more diffuse than those seen in encounters between late-type galaxies.

These effects are illustrated in Fig. 1, which shows the evolution of an off-axis collision between two hot stellar systems. The simulation was performed with an implementation of the Barnes & Hut (1986) hierarchical tree code, using 65,536 particles. The galaxies have a 3:1 mass ratio and are represented by Plummer models. The simulation illustrates the rapid merging of the two bodies, the lack of tidal tails, and the development

Attached as jpeg – full high res pdf  
version of the paper available at  
[www.astro.yale.edu/dokkum/mergers/](http://www.astro.yale.edu/dokkum/mergers/)

FIG. 1.— Illustration of an off-axis collision between hot stellar systems, with mass ratio 3:1. The simulation was performed with an implementation of the Barnes & Hut (1986) tree code, using 65,536 particles. The galaxies merge quickly; after the merger the only morphological signature is the presence of a broad asymmetric fan of material, which rapidly becomes more diffuse. Note the lack of tidal tails, which only form if there is a significant cold component.

of a large fan of material. The central parts of the merger remnant quickly settle in a new equilibrium configuration, whereas the material in the outer parts – where dynamical timescales are long – gradually becomes more diffuse. For a more general analysis of the development of elliptical-elliptical mergers, including the effects of rotation and different mass ratios, we refer to Combes et al. (1995) and subsequent papers.

The surface brightness of tidal features associated with this type of mergers is comparatively low: the features consist of old, red stellar populations, and have higher  $M/L$  ratios than the blue tails associated with mergers of late-type galaxies. Furthermore, they are typically more diffuse, due to the lack of a cold disk in the progenitors. After the merger, the evidence of the past encounter becomes increasingly difficult to detect as dynamical evolution reduces the surface brightness further (e.g., Mihos 1995). No detailed simulations have been done of the expected surface brightness evolution of tidal features resulting from early-type mergers, but a very rough estimate can be obtained from the simulation shown in Fig. 1. Calibrating the output such that the average surface brightness within the effective radius of the remnant  $\langle\mu_R\rangle = 20 \text{ mag arcsec}^{-2}$  (Jørgensen, Franx, & Kjaergaard 1995), we find that the “fan” of material to the upper left has  $\mu_R \sim 25$  at  $t = 10$ , i.e., immediately after the merger. The following timesteps show a continued rapid decrease of the brightness, reaching  $\mu_R \sim 27$  at  $t = 15$ , the final time step of the simulation.

It is difficult to reach such low surface brightness levels observationally: extreme enhancements of photographic plates enabled Malin & Carter (1983) to detect features to  $\mu \sim 26.5$ , similar to the limits reached by Schweizer & Seitzer (1992) with their deep CCD exposures on the Kitt Peak 0.9 m telescope. Detecting features with surface brightness 27–28 requires several hours of integration time on 4 m class telescopes, and to image a sizeable sample of nearby galaxies would require hundreds of hours. Furthermore, flat fielding would have to be accurate to  $\lesssim 0.1\%$  over the entire  $10' - 30'$  field.

These practical difficulties can be solved by exploiting the fact that the  $(1+z)^4$  cosmological surface brightness dimming is a very slow function of redshift for  $z \ll 1$ . Whereas moving a galaxy from  $z = 0.01$  to  $z = 0.1$  reduces its total brightness by 5 magnitudes, its surface brightness changes by only 0.35 mag. In practice it is easier to detect very faint surface brightness features around a galaxy at  $z = 0.1$  than at  $z = 0.01$  as it occupies a  $70\times$  smaller area of the detector. Furthermore, and most importantly, a study of tidal features at  $z \sim 0.1$  does not require a dedicated survey but can be done with existing imaging data.

### 3. DATA

We use data from two deep extra-galactic surveys: the Multiwavelength Survey by Yale-Chile (MUSYC; Gawiser et al. 2005), and the NOAO Deep Wide-Field Survey (NDWFS; Januzzi & Dey 1999, Januzzi et al. 2005, Dey et al. 2005). The data products from the optical imaging components of the two survey are quite similar, as they both use the  $8192 \times 8192$  pixel MOSAIC cameras on the NOAO 4m telescopes. The full dataset covers 10.5 square degrees of sky, reaching  $1\sigma$  surface brightness levels of  $\mu \approx 29 \text{ mag arcsec}^{-2}$ .

#### 3.1. MUSYC

MUSYC is a deep optical/near-infrared imaging and spectroscopic survey of two Southern and two equatorial  $30' \times 30'$

fields, chosen for their low background and the availability of data at other wavelengths. The fields are the Extended Chandra Deep Field South (E-CDFS), the Extended Hubble Deep Field South (E-HDFS), the field centered on the  $z = 6.3$  Sloan Digital Sky Survey quasar SDSS 1030+05 (Becker et al. 2001), and the blank low background field CW 1255+01. The primary goal of the survey is the study of normal and active galaxies at  $z > 2$ .

The survey design and data analysis procedures are described in Gawiser et al. (2005). Briefly, the optical imaging data consist of deep  $UBVRIZ$  exposures obtained with MOSAIC-I on the Mayall 4m telescope on Kitt Peak and MOSAIC-II on the Blanco 4m telescope on Cerro Tololo. The images have a scale of  $0''.267 \text{ pix}^{-1}$ , and typical seeing of  $1''.1$ . The data reach depths of  $\approx 26$  in  $U$ ,  $\approx 26.5$  in  $B$ ,  $V$ , and  $R$ ,  $\approx 25$  in  $I$ , and  $\approx 24$  in  $z$  (AB magnitudes,  $5\sigma$  point source detections), with some variation between the fields. The full exposure time is typically realized over an area of  $33' \times 33'$ , and the total optical survey area is  $1.2 \text{ deg}^2$ .

For detection of low surface brightness features we used the co-added “BVR” images (see Gawiser et al. 2005), which are combinations of the  $B$ ,  $V$ , and  $R$  frames. The total effective integration time of these frames is typically  $\sim 8$  hours. The final depth reaches magnitude  $\approx 27$  (AB;  $5\sigma$  point source detection), with slight variations from field to field.

#### 3.2. NOAO Deep Wide-Field Survey

The NDWFS is a public optical and near-infrared imaging survey over two  $9.3 \text{ deg}^2$  fields: a  $3^\circ \times 3^\circ$  field in Boötes, centered at  $14^h 32^m, +34^\circ 17'$ , and a  $2.3^\circ \times 4^\circ$  field in Cetus, centered at  $2^h 10^m, -4^\circ 30'$  (see Januzzi & Dey 1999; Januzzi et al. 2005). The primary goal of the survey is to study large scale structure at  $z > 1$ . We use the optical images available in the third data release (DR3; October 22 2004). This release comprises the entire  $9.3 \text{ deg}^2$  Boötes field.

Compared to MUSYC, the NDWFS sacrifices multi-band coverage for area. Only three optical filters are used:  $B_w$ ,  $R$ , and  $I$ . The  $B_w$  filter was designed specifically for the NDWFS: it is a very broad blue filter, effectively a combination of the standard  $U$  and  $B$  filters. Exposure times vary across the field; the median values are 8400 s in  $B_w$ , 6000 s in  $R$ , and 11400 s in  $I$ . Details of DR3 can be found on the NDWFS webpages<sup>1</sup>.

The data were not pasted together in a mosaic by NOAO but released as 27 partially overlapping  $35' \times 35'$  MOSAIC pointings. We obtained all 27 pointings in  $B_w$ ,  $R$ , and  $I$  from the NOAO archive. In order to increase the signal-to-noise (S/N) ratio we created co-added “BRI” images, in the following way. First, all images were normalized such that 1 count corresponds to  $AB = 30 \text{ mag}$ . Next, the summed BRI images were created from the  $B$ ,  $R$ , and  $I$  frames according to  $BRI = B + R + 0.5 \times I$ . This procedure optimizes the S/N ratio for objects with the approximate SED of nearby elliptical galaxies.

#### 3.3. Depth of Summed Images

The detection of diffuse tidal features depends on the limiting surface brightness level of the data, not on the point source detection limit. To assess the (AB) surface brightness limits we placed random apertures with an area of  $1''$  in empty regions, and determined the rms fluctuations. The co-added images were used, i.e., the “BVR” images for MUSYC and the “BRI” images for NDWFS.

<sup>1</sup> <http://www.noao.edu/noao/noadeep/DR3/>

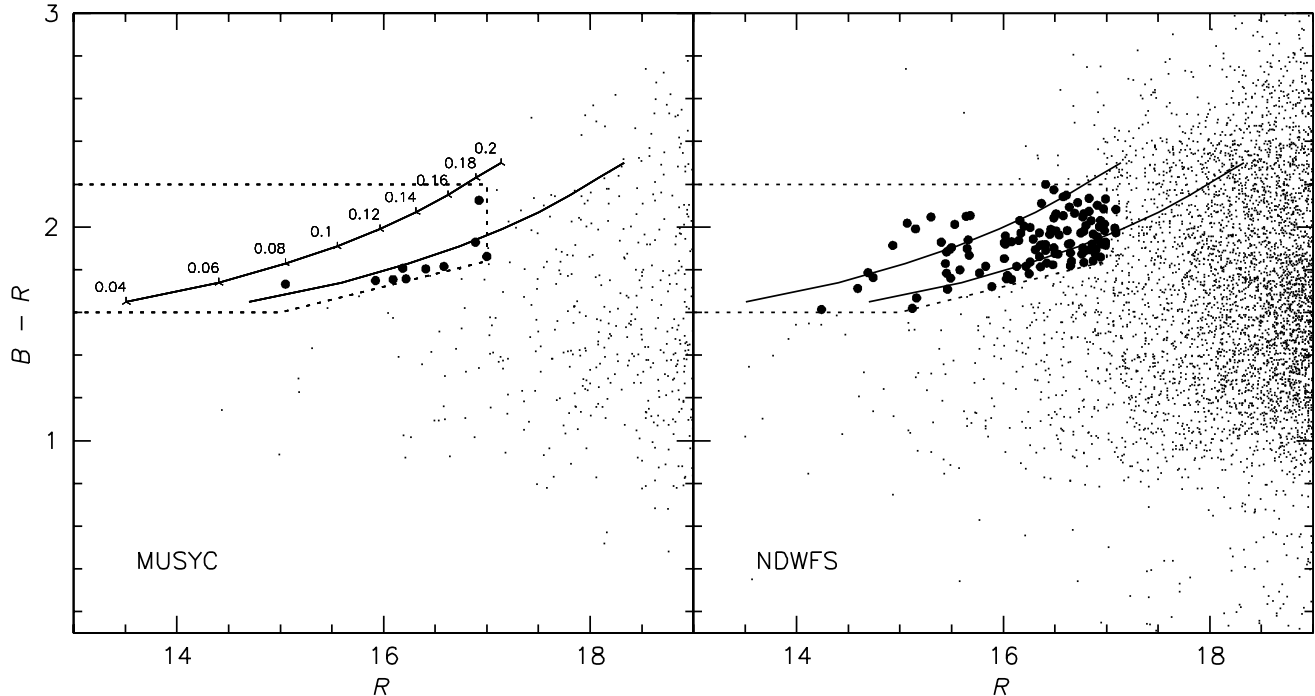


FIG. 2.— Sample selection. Solid lines show the expected  $B-R$  colors and  $R$  magnitudes for  $L_*$  and  $3L_*$  elliptical galaxies at redshifts  $0.04 \leq z \leq 0.20$ . The dashed lines shows the selection region in color and magnitude. MUSYC consists of four  $0.3 \text{ deg}^2$  fields, including the areas around the Chandra Deep Field South and the Hubble Deep Field South. The NDWFS covers a contiguous area of  $9.3 \text{ deg}^2$ .

The MUSYC images have a typical  $1\sigma$  surface brightness limit of  $\mu \approx 29.5 \text{ mag arcsec}^{-2}$  whereas this limit is  $\approx 29 \text{ mag arcsec}^{-2}$  for the NDWFS images. These numbers are approximate: the exact limit depends on the field, the local flat fielding accuracy, and on the assumed spectral energy distribution of the source. The greater depth of MUSYC was expected, as more exposure time was devoted to the efficient  $B$ ,  $V$  and  $R$  filters.

The ability to detect low surface brightness emission is influenced by the extent of the features, confusion with neighboring objects, the contrast with the smooth emission from the galaxy, and other effects; in practice, we find we can confidently identify features down to  $\mu \approx 28 \text{ mag arcsec}^{-2}$ .

#### 4. SAMPLE SELECTION

The initial sample selection is based on color and magnitude only. No morphological criteria are applied, for three reasons: first, a simple color cut is straightforward to reproduce; second, as the galaxies are typically at  $z \sim 0.1$  it can be difficult to determine morphologies from ground-based data (see § 5.1); and third, the classification process itself might bias the sample toward or against galaxies with tidal features.

##### 4.1. Catalogs

The combination of the two surveys comprises 31 multi-band tiles, each covering  $\approx 0.3 \text{ deg}^2$ . Catalogs were created using the SExtractor software (Bertin & Arnouts 1996). SExtractor catalogs were available for both surveys but these are optimized for faint point sources, not for large, nearby galaxies. SExtractor was run with its default settings, with the following changes. The detection threshold was set at  $20\sigma$ , with the added requirement that 10 adjacent pixels are above the threshold, and the mesh size for background subtraction was set at 400 pixels rather than the default 64 to avoid oversubtraction of

the background for large galaxies. Matched photometry in each band was obtained by running SExtractor in dual image mode, always using the  $R$ -band images for detection.

SExtractor's AUTO magnitudes are used as best estimates for total magnitudes. Colors were initially determined in fixed  $5''$  diameter apertures. However, we find that colors measured in fixed apertures are not well suited for these large objects as they introduce distance-dependent selection biases. Specifically, when selecting on aperture color the sample invariably contains large, presumably very nearby spiral galaxies with blue disks and red bulges. In the following,  $B-R$  colors refer to  $B_{\text{AUTO}} - R_{\text{AUTO}}$ , measured in dual image mode.

Finally, the measured  $B_w - R$  colors in the NDWFS are converted to the standard Johnson system. The  $B_w$  filter has a bluer central wavelength than the  $B$  filter, which means  $B_w - R$  colors are significantly redder than standard  $B - R$  colors. Using templates from Coleman, Wu, & Weedman (1980) we derive

$$(B-R) = 0.27 + 0.62(B_w - R) + 0.07(B_w - R)^2. \quad (1)$$

This transformation holds to a few percent for  $1 < (B-R) < 2.5$  and redshifts  $z < 0.2$ , and was applied to the NDWFS photometry prior to the sample selection. Total magnitudes and colors are given on the Vega system to facilitate comparisons to previous studies.

##### 4.2. Color Selection

Galaxies are selected on the basis of their total  $R$  magnitude and  $B-R$  color. Figure 2 shows color-magnitude diagrams for the four MUSYC fields (left) and for the 27 NDWFS fields (right). Only objects with a star/galaxy classification  $< 0.06$  are shown (see Bertin & Arnouts 1996). This classification is fairly robust at the magnitudes of interest, and effectively removes both non-saturated and saturated stars from the sample. Visual inspection revealed that the software assigned a

star/galaxy classification  $\geq 0.06$  to four galaxies in our sample; for these objects the value was manually set to zero. We note that the cores of some bright galaxies can be saturated, which influences the magnitudes and (particularly) the colors in unpredictable ways. As this effect is difficult to quantify and only influences a handful of objects we did not attempt a correction. The distribution of points is similar in the two surveys. The number of objects in the NDWFS is an order of magnitude larger than in MUSYC, as expected from the difference in area.

We selected galaxies with the colors and magnitudes of  $L > L_*$  early-type galaxies at  $0.05 < z < 0.2$ . The two solid lines show the colors of the Coleman et al. (1980) E/S0 template redshifted from  $z = 0.04$  to  $z = 0.20$ , normalized to  $L_*$  and  $3L_*$  (Blanton et al. 2001). Dashed lines delineate the adopted selection region:  $R < 17$ ,  $1.6 \leq (B - R) \leq 2.2$ , and  $(B - R) > 1.6 + 0.12 \times (R - 15)$ . The galaxies in the dashed region are the brightest and reddest in 10.5 square degrees of sky.

#### 4.3. Additional Steps

After visual inspection of the initial sample of 155 red objects 32 were removed for various reasons. The discarded objects fall in a wide range of categories: mis-classified stars (usually blends with other stars or galaxies); objects on the edge of a field; spurious objects (always near very bright stars); severely saturated galaxies (although interesting in their own right, as they are likely very bright active nuclei); and galaxies that have more than one catalog listing. The latter occurs because the 27 NDWFS tiles have some overlap; in these cases the data from the overlapping pointings were added, unless the S/N is much higher in one of the two. We also removed 12 galaxies that are likely members of known galaxy clusters. Eight are located within  $8'$  of NSC J142841+323859, a cluster at  $z = 0.127$ , and four are located within  $4'$  of the poorer, more compact cluster NSC J142701+341214 at  $z \approx 0.2$  (Gal et al. 2003).

Finally, we inspected all galaxies with  $17 \leq R \leq 17.75$  to identify merging pairs (see § 5.2) that are split into two objects by SExtractor, and whose *combined* luminosities and colors would place them in our selection region. Three such pairs were identified, and the brightest galaxy of each pair was added to the sample: 4-1190, 4-1975, and 22-2252. The final sample thus consists of 126 red field galaxies in MUSYC and the third data release of the NDWFS.

#### 4.4. Median Redshift

The median  $R$  magnitude of galaxies in our sample is 16.4, and the median  $B - R$  color is 1.92. As can be seen in Fig. 2 these values suggest that the median galaxy is an  $L \approx 1.2L_*$  early-type galaxy at redshift  $z \approx 0.11$ . Currently we have redshifts for only nine of the 123 galaxies: four in the CDF-S from COMBO-17 (Wolf et al. 2005), two in the SDSS 1030+05 field from the SDSS (York et al. 2000), and three in the CW 1255+01 field from the SDSS. The mean redshift of these nine objects  $\langle z \rangle = 0.13$  with a spread of 0.02, consistent with the expectations from our color selection.

As a further test on the selection we obtained photometric and spectroscopic data in ten randomly selected  $3^\circ \times 3^\circ$  fields from the SDSS. Galaxies were selected in the  $g - r$  vs.  $r$  plane in the same manner as in our study, using the Fukugita et al. (1995) transformations to convert our  $R$  and  $B - R$  limits to SDSS  $r$  and  $g - r$  limits. The median redshift is 0.098, with 90 % of the galaxies at  $z > 0.05$ . The rms field-to-field variation of the median is only 0.008.

In the following we will adopt  $z = 0.1$  as the median redshift; our conclusions change very little if we were to use, e.g.,  $z = 0.08$  or  $z = 0.13$  instead. For  $z \approx 0.1$  our observed  $R$ -band limit corresponds to  $M_R \sim -21$ , and the median galaxy has  $M_R \sim -22$ .

## 5. ANALYSIS

### 5.1. Morphologies

All galaxies were assigned a morphological type by visually inspecting their summed images (i.e., the “BVR” images for MUSYC galaxies and the “BRI” images for NDWFS objects). The images span a large range in surface brightness levels, going from the nearly saturated central regions to very low surface brightness features up to  $> 50$  kpc away from the center. As the relevant dynamic brightness range is  $\gtrsim 10^4$  each galaxy was displayed at four different contrast levels simultaneously.

The morphological types are necessarily broad. Although the S/N ratio is very high the spatial resolution is quite poor: the typical seeing is  $1''.1$ , which corresponds to 3 kpc at  $z = 0.1$ . Therefore, we only have 2 – 3 resolution elements within the half-light radii of many galaxies (see, e.g., Jørgensen, Franx, & Kjaergaard 1995). The assigned types are spiral (S), indicating the presence of spiral arms and/or star forming regions in a disk; S0, indicating an early-type galaxy with an unambiguous disk component; and E/S0, indicating a bulge-dominated early-type galaxy. We cannot securely separate elliptical galaxies from bulge-dominated or face-on S0 galaxies. Contrary to the usual definition the E/S0 class therefore encompasses ellipticals, bulge-dominated S0s, E/S0s, and S0/Es.

Morphological classifications are listed in Table 1, and images of all 126 galaxies are shown in the Appendix. As expected, the sample is dominated by early-type galaxies: of 126 objects, 10 (8 %) are classified as spirals, 30 (24 %) as S0s (i.e., disk-dominated early-type galaxies), and 86 (68 %) as E/S0s (i.e., bulge-dominated early-type galaxies). Most of the spiral galaxies have large red bulges and faint blue arms. Based on their morphologies at surface brightness levels  $\mu \lesssim 25$  mag arcsec<sup>2</sup> we infer that virtually all galaxies in our sample are red because of their evolved stellar populations, and not because of dust (as is well known from many previous studies of bright red galaxies in the local Universe; see, e.g., Sandage & Visvanathan 1978, Strateva et al. 2001).

### 5.2. Tidal Features

Tidal features were first identified by visual inspection of the full sample of 126 galaxies; a quantitative analysis of disturbances in the restricted sample of 86 bulge-dominated early-type galaxies follows in § 5.3. The flag describing tidal features can have one of four values: 0 for no tidal features, 1 for weak features, 2 for strong features, and 3 for an ongoing interaction with another galaxy. Galaxies in the “2” class are generally highly deformed merger remnants, whereas the “1” class indicates more subtle features. The difference is obviously quite subjective, and in the subsequent analysis these two classes will generally be combined into one. A “3” classification implies that both the primary and secondary galaxy show clear distortions or tidal tails.

The key result of our analysis is the ubiquity of tidal features, particularly among bulge-dominated early-type galaxies. In the full sample of 126 galaxies, 44 (35 %) show clear signs of past interactions and in an additional 23 cases (18 %) the interaction is still in progress. Only 59 galaxies (47 %) appear

Attached as jpeg – full high res pdf  
 version of the paper available at  
[www.astro.yale.edu/dokkum/mergers/](http://www.astro.yale.edu/dokkum/mergers/)

FIG. 3.— Examples of red mergers, ordered by the progression of the interaction. The images were generated by combining the *B* and *R* frames. The objects are 17-596 and 17-681 (a); 19-2206 and 19-2242 (b); 1256-5723 (c); and 16-1302 (d). Panel (a) spans  $5' \times 5'$ ; panels (b), (c), and (d) span  $2'.5 \times 2'.5$ . The tidal features are faint and red, and generally barely visible in *B*. Similar features are seen in a large fraction of our sample of 123 red galaxies, in particular among the bulge-dominated early-type galaxies. Images of all objects are given in the Appendix.

undisturbed, showing no unambiguous tidal features at the surface brightness limit of the survey. The fraction of disturbed objects is lowest among galaxies with a clear disk component. Among 40 galaxies classified as S or S0, only six (15 %) show evidence for past or present interactions. In contrast, among the 86 galaxies classified as E/S0 undisturbed objects are the exception, as 61 (71 %) show tidal features.

The nature and extent of the disturbances span a wide range. Some galaxies have clearly defined tidal tails while others show

broad fans of stars similar to the final frames of the simulation shown in Fig. 1. In most cases the disturbances are subtle and only visible at large radii and very faint surface brightness levels, although some objects are strongly disturbed throughout. Often we see a mixture, e.g., a well defined tail in addition to a broad, smooth disturbance at very faint levels. This large range of properties is not surprising as it reflects the variation in the age of the interaction, the viewing angles, and the properties of the progenitors.

Attached as jpeg – full high res pdf  
 version of the paper available at  
[www.astro.yale.edu/dokkum/mergers/](http://www.astro.yale.edu/dokkum/mergers/)

FIG. 4.— Same as Fig. 3, but now highlighting faint surface brightness levels in the summed exposures. The four systems have extensive tidal debris, extending to  $1'$  or more from the center. Features can be reliably detected down to  $\sim 28 \text{ mag arcsec}^{-2}$ . Despite their large extent the features contain less than 10 % of the total light of the galaxies.

The tidal features are almost always red. In many cases the features are only visible in the *R* and *I* frames despite the substantial depth of the blue exposures. They also appear smooth, showing no or very little evidence for clumps and condensations. In these respects the features are very different from the blue, clumpy tidal tails seen in spiral–spiral interactions (e.g., Mirabel, Dottori, & Lutz 1992; Hunsberger, Charlton, & Zaritsky 1996), and from the sharp shells and ripples detected in unsharp-masked images of ellipticals (e.g., Schweizer & Seitzer 1992, Colbert et al. 2001). We note here that our data

are not well suited to identify narrow features, as the FWHM resolution of our data is about 2 kpc at  $z = 0.1$ .

The remarkable nature of these red mergers and their remnants is illustrated in Fig. 3. The figure shows two examples of ongoing mergers, an example of a strongly disturbed merger remnant, and an example of a galaxy with more subtle distortions at faint surface brightness levels, arranged in a plausible red merger sequence. In all cases the tidal features are smooth and red, and quite different from the highly structured blue tails associated with known mergers between gas rich disk galaxies.

Figure 4 shows summed images of the same objects, highlighting the faintest features and providing an indication of the surface brightness levels reached by the observations. We stress that these objects are fairly typical examples: as can be inferred from the smaller images shown in the Appendix they are by no means unique within our sample.

### 5.3. Quantitative Identification of Tidal Features

Quantitative characterization of the tidal features is important for testing the robustness of the visual classifications, measuring the flux associated with the features, assessing the effects of changing the S/N ratio, and examining correlations between distortions and other properties of the galaxies. Quantitative criteria are also useful as a tool for future studies of larger samples. Standard measures of asymmetry (e.g., Abraham et al. 1996; Conselice et al. 2003) are not applicable to these galaxies as the features comprise only a small percentage of the total luminosity of the galaxies. Instead a method was developed which determines distortions with respect to a model light distribution (see, e.g., Colbert et al. 2001). The method is only meaningful for bulge-dominated early-type galaxies, which make up the bulk of the sample.

First, the galaxies are fitted by an elliptical galaxy model using the “ellipse” task in IRAF, in three iterations. After each

iteration a mask file is updated using the residuals from the previous fit. The center position, ellipticity, and position angle are allowed to vary with radius. In cases where a second galaxy overlaps the primary object the two objects are fitted iteratively. The final model image is denoted  $M$ . Next, a “clean” galaxy image  $G$  is produced in the following way. Objects bluer or redder than the primary galaxy are masked, by dividing the  $R$  and  $B$  band images, median filtering, and identifying pixels deviating more than a factor two from the median color of the galaxy. To remove small foreground and background objects and retain the smooth galaxy light a “reverse” unsharp masking technique is used: the galaxy images are compared to Gaussian-smoothed versions of themselves, and pixels deviating more than a factor two are masked (excluding the galaxy centers). Pixels in the vicinity of masked pixels are also masked. Finally, a fractional distortion image  $F$  is created by dividing  $G$  by  $M$ . The distortion image is convolved with a  $5 \times 5$  median filter to reduce pixel-to-pixel variations. The parameter  $t$  describing the level of distortion is defined as

$$t = \overline{|F_{x,y} - \overline{F_{x,y}}|}, \quad (2)$$

The tidal parameter thus measures the median absolute deviation of the (fractional) residuals from the model fit.

The procedure is illustrated in Fig. 5, for a galaxy pair with no visible distortions, a galaxy with a weak tidal feature, and a

Attached as jpeg – full high res pdf

version of the paper available at

[www.astro.yale.edu/dokkum/mergers/](http://www.astro.yale.edu/dokkum/mergers/)

FIG. 5.— Illustration of the derivation of  $t$ , the quantity describing the deviations from ellipse fits to the galaxies. Three galaxies are shown: 7-1818 (top) has no visually detected features; 18-794 (center) has a weak tidal feature, and 1256-5723 (bottom) has strong tidal features. From left to right are shown: the summed galaxy image; the galaxy image  $G$  with sharp features, blue features, and low S/N regions masked; the elliptical model fit  $M$ ; and the median-filtered, noise-corrected distortion image  $F$  from which  $t$  is measured.



strongly disturbed object. The visually identified tidal features are isolated and emphasized in the distortion images  $F$  shown at right. The corresponding values of  $t$  vary from 8 % for the undistorted object to 24 % for the strongly disturbed object.

In Fig. 6(a) the values of  $t$  are compared to the visual tidal classifications for all 86 bulge-dominated early-type galaxies. There is a strong correlation: the median value of  $t$  is 0.08 for galaxies classified as undisturbed, 0.13 for weakly disturbed galaxies, and 0.19 for strongly disturbed galaxies and ongoing mergers. Tidal features are usually visually identified if  $t > 0.1$ : of 23 galaxies with  $t < 0.1$  only 5 (22 %) were visually classified as tidally distorted, compared to 56 out of 63 galaxies with  $t \geq 0.1$  (89 %). We conclude that the visually identified distortions are robust and imply median absolute deviations from an ellipse fit of  $\gtrsim 10$  %.

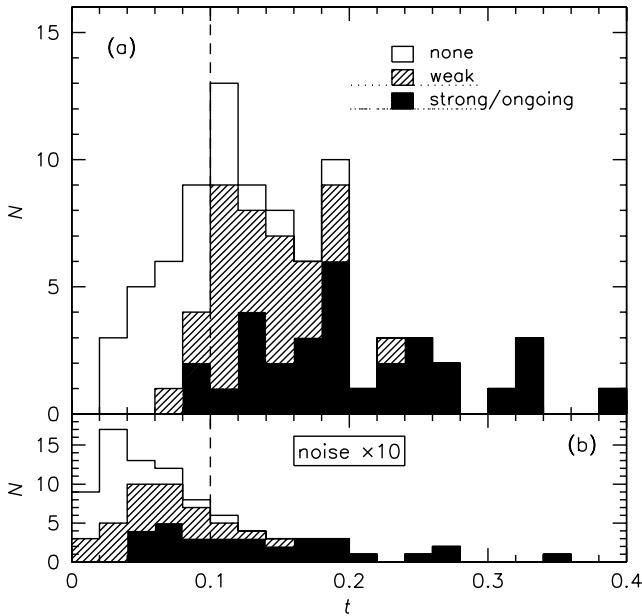


FIG. 6.— Comparison of visual classifications and the tidal parameter  $t$  for the 86 galaxies classified as E/S0. There is a strong correlation between  $t$  and the visual classifications. Galaxies with visually identified tidal features generally have  $t > 0.1$ . The histograms in (b) show the effect of lowering the S/N ratio by a factor ten. The majority of galaxies move to  $t < 0.1$ , and hence would not be identified as tidally distorted objects.

The distortion maps  $F$  can be used to estimate the amount of star light associated with the tidal features. Visual inspection of the distortion maps suggests that pixels deviating more than 15 % from the model are usually associated with visible features. A mask  $F'$  was created by setting pixels with values  $\geq 0.15$  in  $F$  to 1 and all other pixels to zero. The relative flux in the tidal features was then estimated as follows:

$$f_t = \frac{\sum F'_{x,y} \times (G_{x,y} - M_{x,y})}{\sum M_{x,y}}, \quad (3)$$

with the summations over all pixels  $x, y$ . As expected, the median value of  $f_t$  is low for the 25 E/S0 galaxies with  $t < 0.1$ : 0.01, about 1 % of the galaxy light. The median is 0.04 for the 63 galaxies with  $t \geq 0.1$  and 0.07 for the 14 most disturbed galaxies with  $t \geq 0.2$ . From varying the cutoff in  $F$  the systematic uncertainty in these values is estimated at  $\sim 30$  %. We infer that – despite their large extent – the tidal features typically contain only about 5 % of the total light of the galaxies.

#### 5.4. Ongoing Mergers

There are 23 galaxies in the sample that show a clear tidal connection to a secondary object. In four cases the secondary object is also in the sample of 126, leaving nineteen unique systems. The fact that tidal features have developed implies that dynamical friction is already at work. Assuming that the galaxies were initially on nearly parabolic orbits, which is a reasonable assumption for field galaxies, the implication is that virtually all these galaxies will eventually merge (J. Barnes, private communication). We note that our selection of merger pairs by tidal features is different from “standard” photometric and spectroscopic selection of close pairs, where the number of mergers is always smaller than the number of close pairs (e.g., Patton et al. 2002): as expected, there are several close pairs in our sample which do not show tidal features and are not classified as ongoing mergers (see, e.g., the top panels of Fig. 5).

The 19 merger systems are shown in Fig. 7; color images of these objects are in the Appendix, along with all other galaxies. In most cases the primary galaxy is in the sample of 126 and the secondary galaxy is not (because it has  $R > 17$ ). In cases where both galaxies are in the sample, and in cases where the primary galaxy has a double nucleus, we designated the brightest object or nucleus as the primary object. The primary galaxies in the merging pairs are equally bright as other galaxies in the sample: their median  $R$  magnitude is 16.3, compared to 16.4 for the full sample of red galaxies.

The merger sample comprises objects connected by a tidal “bridge” (e.g., 1-2874, 5-2345, 18-485/522); double nuclei in a highly disturbed common envelope (cdfs-374, cdfs-1100, 4-1190, 11-962); and objects of similar brightness with disturbed isophotes and tidal tails or fans (e.g., 2-3070/3102, 4-1975, 7-4247, 17-596/681, 19-2206/2242). Visual inspection of the merging systems indicates that the mergers are usually not between blue, disk-dominated systems but between red, bulge-dominated systems. Furthermore, in many cases the secondary galaxy appears to be of similar brightness as the primary galaxy. Eight of the 126 galaxies are merging with each other: the four bright, red pairs are 2-3070/3102, 17-596/681, 18-485/522, and 19-2206/2242.

We quantified these effects in the following way. The luminosity ratio is defined as

$$\frac{L_2}{L_1} = 10^{(R_1 - R_2)/2.5}, \quad (4)$$

and the color difference as

$$\Delta(B - R) = (B_2 - R_2) - (B_1 - R_1). \quad (5)$$

In the 16 cases where the primary and the secondary galaxy are both in the SExtractor catalog we calculated the luminosity ratio and the color difference directly (see § 4.1). In three cases the pair is too close to be separated into two objects by SExtractor (cds-374, cdfs-1100, and 11-962). These objects are perhaps better described as single galaxies with double nuclei. Photometry for the nuclei was obtained from aperture photometry, with the radius of the aperture equal to half the distance between the nuclei. We note that the double nucleus of 11-962 is elongated but unresolved in the NDWFS images: the enlarged image shown in Fig. 7 was obtained with the OPTIC camera (Tonry et al. 2005) on the WIYN telescope, and has a resolution of  $0''.45$  FWHM.

As a check on the robustness of the results we also obtained aperture photometry in fixed  $5''$  apertures for the 16 pairs that

Attached as jpeg – full high res pdf  
version of the paper available at  
[www.astro.yale.edu/dokkum/mergers/](http://www.astro.yale.edu/dokkum/mergers/)

FIG. 7.— The nineteen ongoing mergers in the red galaxy sample. The center of 11-962 is unresolved at the resolution of the NDWFS, and the image showing the two nuclei was obtained with the WIYN telescope in  $0''.45$  seeing. Note that in four cases both the primary galaxy and its companion are in the  $R < 17$  red galaxy sample. In three cases (4-1190, 4-1975, and 22-2252) the individual paired galaxies are fainter than  $R = 17$  but their combined luminosity exceeds this limit.

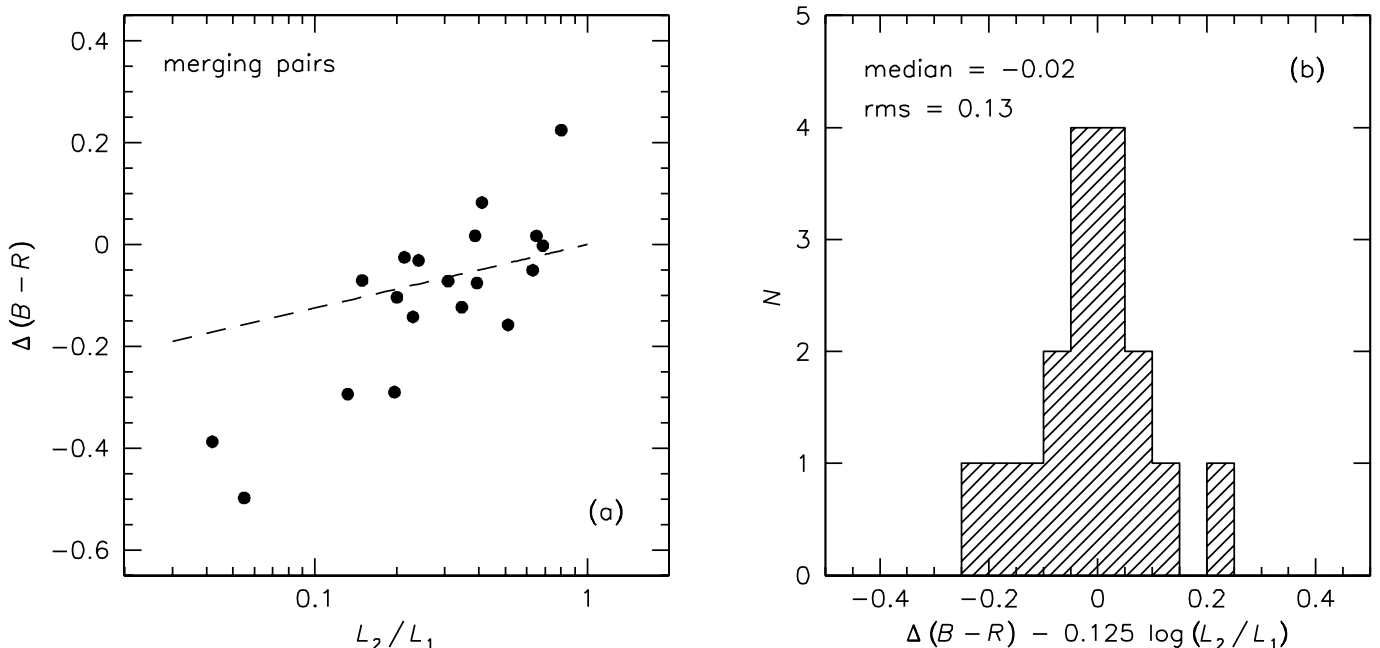


FIG. 8.— Luminosity ratios and color differences of the 19 interacting pairs. The median luminosity ratio is 0.31, and the median color difference is  $-0.07$ . Panel (a) shows that the color difference correlates with the luminosity ratio, in the sense that faint companions are bluer. The broken line is the correlation expected for early-type galaxies on the color-magnitude relation. Color differences are plotted in (b), after removing this relation. The median residual color difference is  $-0.02$ , with a scatter of 0.13 magnitudes.

are well separated. This method underestimates the luminosity differences, as the secondary galaxies are usually more compact than the primary galaxies. Nevertheless, the results are very similar, giving a median luminosity ratio that is only  $\sim 20\%$  higher than derived from the SExtractor AUTO magnitudes.

The pair photometry is given in Table 1. Luminosity ratios range from 0.04 to 0.80, i.e., from relatively minor 1:25 accretion events to nearly equal mass mergers. The median luminosity ratio is 0.31, or a 1:3 merger. We conclude that approximately half the ongoing interactions are major mergers. The median color difference is only  $-0.07$ , i.e., companions are typically 0.07 magnitudes bluer than the primary galaxy. As the companions are (by definition) fainter than the primary galaxies, this small difference may be an effect of the existence of the color-magnitude relation. Figure 8(a) shows the relation between color difference and luminosity ratio. There is a correlation, with the faintest companions being the bluest. The dashed line shows the expected correlation for elliptical galaxies on the (galaxy cluster) color-magnitude relation (López-Cruz, Barkhouse, & Yee 2004). In Fig. 8(b) we show the distribution of residual color differences after subtracting this relation. The median of the distribution is  $-0.02$  and the rms scatter is only 0.13 magnitudes.

These results show that the ongoing mergers in our sample occur “within” the red sequence with very small scatter. This result cannot be attributed to our selection criteria: as 16 of the 19 pairs are separated by SExtractor there is no obvious bias against detecting blue companions to the primary galaxies. There is a hint that the observed relation in Fig. 8(a) is steeper than expected from the color-magnitude relation, but this is largely due to the two pairs with  $L_2/L_1 \approx 0.05$  and the spiral/S0 merger 18-485/522. Among pairs with  $L_2/L_1 > 0.1$  whose primary galaxy is classified as early-type the residual scatter in  $\Delta(B-R)$  is only 0.08 magnitudes.

TABLE 1  
PHOTOMETRY OF MERGER PAIRS

Object	$L_2/L_1$	$\Delta(B-R)$
cdfs-374	0.39	$-0.08$
cdfs-1100	0.35	$-0.12$
cdfs-6976	0.23	$-0.14$
1-2874	0.05	$-0.50$
2-3070	0.63	$-0.05$
4-1190	0.39	0.02
4-1975	0.51	$-0.16$
4-2713	0.13	$-0.29$
5-2345	0.04	$-0.39$
7-4247	0.21	$-0.03$
11-962	0.69	$-0.00$
11-1278	0.15	$-0.07$
11-1732	0.20	$-0.29$
14-1401	0.24	$-0.03$
17-596	0.65	0.02
18-485	0.80	0.22
19-2206	0.41	0.08
22-2252	0.31	$-0.07$
26-2558	0.20	$-0.10$

## 6. DISCUSSION

### 6.1. Why Were They Missed?

The key results of our analysis are the large number of ongoing red mergers and the ubiquity of tidal features associated with (in particular) bulge-dominated early-type galaxies (galaxies classified as “E/S0”). As discussed in § 5.2 the large scale, low surface brightness features that we see are different from the ripples and shells that have been reported previously in unsharp-masked images of ellipticals at  $z \sim 0$ . Our sample is essentially local, in the sense that the merger rate is not expected to evolve significantly from  $z \sim 0.1$  to  $z \sim 0$ . Nearby galaxies have been studied in great detail over the past decades,

and before discussing the consequences of our findings we address the question why this preponderance of smooth red tidal features has not been seen before.

The subjective nature of the visual classifications can be ruled out as a cause given the consistency of visual and quantitative classifications: 73 % of E/S0 galaxies have  $t > 0.1$ . Small number statistics also play a minor role given the large number of objects in the sample. Given the fact that more than 90 % of the sample comes from the NDWFS we cannot rule out that the fraction of interacting galaxies is unusually high in that region of the sky. Random  $3^\circ \times 3^\circ$  SDSS fields (see § 4.4) show substantial peaks in the redshift distribution within each field, reflecting the fact that most red galaxies live in groups and filaments. We note, however, that the red galaxies are distributed rather uniformly over the NDWFS area, and that some of the most spectacular mergers are in the unrelated MUSYC fields.

The most likely reason why the ubiquity of red mergers in the local universe was missed so far is the depth and uniformity of the available imaging. Classic imaging studies of nearby elliptical galaxies (e.g., Franx, Illingworth, & Heckman 1989; Peletier et al. 1990) used exposure times in the red of only 180 s – 600 s on 1 m – 2 m class telescopes, and such short exposures have been the norm ever since (e.g., Zepf, Whitmore, & Levison 1991; Pildis, Bregman, & Schombert 1995; Jansen et al. 2000; Colbert et al. 2001). Similarly, the effective exposure time of the Sloan Digital Sky Survey is about 51 s per filter (York et al. 2000).

Among the deepest imaging surveys are those of Malin & Carter (1983), who performed extreme enhancements of photographic plates to bring out low surface brightness features, and Schweizer & Seitzer (1992), who used 2400 s – 3600 s integrations with the 0.9 m telescope on Kitt Peak. These studies reach AB surface brightness limits of  $\mu \sim 26.5$  mag arcsec $^{-2}$ . Although both studies find sharp distortions in the form of ripples and shells in a large fraction of ellipticals, their depth and field-of-view are not sufficient to find the large low surface brightness features that we report here. The exposure time that went into each of the images discussed here is  $\approx 27,000$  s on 4 m class telescopes equipped with modern CCDs (equivalent to 120 hours on a 1 m class telescope), and to our knowledge such long exposures have never been obtained of a significant sample of nearby red galaxies.

Figure 9 shows what Fig. 4 would look like if we had exposed for 600 s on a 1 m class telescope. Very little remains of the dramatic tidal features evident in Fig. 4, illustrating the extreme depth of the NDWFS and MUSYC surveys. We quantified the effect of the S/N ratio on the detectability of tidal features by artificially increasing the noise in our images by a factor of ten, corresponding to a decrease in exposure time of a factor of 100. The degraded images are of similar depth as those of Malin & Carter (1983) and Schweizer & Seitzer (1992), and are still substantially deeper than virtually all other imaging studies of nearby elliptical galaxies. As shown in Fig. 6(b) the distribution of  $t$  changes substantially when the S/N is decreased. Only 29 % of E/S0s in the degraded images have  $t > 0.1$ , compared to 73 % in the original images.

We conclude that the high incidence of tidal features in our sample is a direct consequence of the faint surface brightness levels reached by the data. We also note that flat fielding uncertainties may prohibit the detection of broad tidal features around local galaxies irrespective of exposure time. The faint debris in Fig. 4 has a very large extent in comparison to the

high surface brightness regions visible in Fig. 9, and moving the galaxies to  $z \sim 0.01$  would change the surface brightness very little but increase the sizes of the debris fields to  $\sim 10'$  or more. Finally, galaxy surveys in blue filters (e.g., Arp 1966) would classify the majority of objects in our sample as undisturbed even if they met the surface brightness and flat fielding requirements.

Attached as jpeg – full high res pdf

version of the paper available at

[www.astro.yale.edu/dokkum/mergers/](http://www.astro.yale.edu/dokkum/mergers/)

FIG. 9.— Simulated appearance of the galaxies in Figs. 3 and 4 if observed for 600 s on a 1 m class telescope, a typical imaging depth for studies of nearby bright galaxies. Owing to its low surface brightness the large scale tidal debris is all but invisible. For comparison, the contour outlines the  $\mu \approx 27.5$  mag arcsec $^{-2}$  level in Fig. 4.

## 6.2. Recent Merger History of Bulge-Dominated Galaxies

We first determine the implications of the observed interactions only, without applying corrections for the short duration of the mergers. We define a sample which contains both current and future bulge-dominated galaxies, consisting of the 86 bulge-dominated galaxies (classified as E/S0), minus half of the six E/S0s which are interacting with each other, plus the disk-dominated galaxies (classified as S or S0) which are involved in a major merger. Among disk-dominated galaxies the only major merger is the spiral/S0 pair 18-485/522, whose constituent galaxies have roughly equal luminosity. The total sample of current and future bulge-dominated galaxies is therefore  $86 - 3 + 1 = 84$ . Among this sample of 84 galaxies there are eighteen current mergers and 41 remnants, and we infer that 70 % of current and future bulge-dominated galaxies experienced a merger or accretion event in the recent past.

The red ongoing mergers and the red tidal features associated with many of the E/S0 galaxies very likely sample the same physical process at different times. On average, galaxies with strong tidal features are probably observed shortly after the merger and galaxies with weak features are observed at later times. Assuming that the ongoing mergers are representative for the progenitors of all remnants we can directly infer the mass ratios of the progenitors of the full sample of 59 current and future bulge-dominated early-type galaxies. The median luminosity ratio of the ongoing mergers is 0.31, and the me-

dian color difference is negligible after correcting for the slope of the color-magnitude relation. Assuming that  $M/L \propto M^{0.2}$  (e.g., Jørgensen et al. 1996) a luminosity ratio of 0.31 implies a median mass ratio of 0.23, or a 1:4 merger.

There is also indirect evidence that the progenitors of the remnants were typically major mergers rather than low mass accretion events. Simulations by Johnston, Sackett, & Bullock (2001) show that surface brightness levels  $28 < \mu < 33$  are typical for the debris of small satellites such as the Local Group dwarfs. Similarly, the average surface brightness of the giant stream of M31 is  $\mu_V \approx 30 \text{ mag arcsec}^{-2}$  (Ibata et al. 2001) and that of the debris from the Sagittarius dwarf  $\mu_V \approx 31 \text{ mag arcsec}^{-2}$  (Johnston et al. 2001). All these values are well beyond the detection limit of our survey. Furthermore, the fraction of tidally disturbed galaxies is much lower among disk-dominated galaxies than among bulge-dominated galaxies. Ignoring the ongoing mergers only 8% of disk-dominated galaxies show tidal features compared to 62% of bulge-dominated galaxies. This difference is consistent with the idea that the events responsible for the tidal features were usually sufficiently strong to disturb any dominant disk component. Finally, the fact that the features are typically broad and red suggests that the progenitors were dynamically hot systems with old stellar populations, consistent with the properties of the galaxies in the ongoing mergers. We also note that the fraction of light associated with the features ( $\sim 5\%$ ) is very similar to the fraction of light associated with the tidal debris in the 1:3 merger simulation shown in Fig. 1.

We conclude that approximately 35% of bulge-dominated red galaxies experienced a major merger with mass ratio  $> 1:4$  in the time window probed by our observations. This result is direct observational confirmation of the hierarchical assembly of massive galaxies.

### 6.3. Merger Rate and Mass Accretion Rate

Up to this point the analysis did not require an estimate of the timescale of the mergers. Such estimates are obviously uncertain, but they are necessary for turning the merger fraction into a merger rate and a mass accretion rate. These numbers are more easily compared to models and other observational studies, and are needed for extrapolating the results to higher redshifts.

The merger rate can be defined in a variety of ways (see, e.g., Patton et al. 2002). Here it is expressed as the number of remnants that are formed per Gyr within our selection area:

$$R = \frac{f_m}{t_m} \text{ Gyr}^{-1}, \quad (6)$$

with  $f_m$  the fraction of the galaxy population involved in a merger – with pairs counted as single objects – and  $t_m$  a characteristic timescale for the mergers. We restrict the analysis to the sample of nineteen ongoing mergers, as simulations of the fading of tidal debris around the remnants of dry mergers have not yet been done in a systematic way.

Following Patton et al. (2000) we assume that the timescale of the mergers can be approximated by the dynamical friction timescale, given by

$$T_{\text{fric}} = \frac{2.64 \times 10^5 r^2 v_c}{M \ln \Lambda} \text{ Gyr}, \quad (7)$$

where  $r$  is the physical separation of the pairs,  $v_c$  is the circular velocity,  $M$  is the mass of the lowest mass galaxy, and  $\ln \Lambda$  is the Coulomb logarithm (see Binney & Tremaine 1987; Patton et al. 2000). The median projected separation of the paired

galaxies is  $8''.6$ , or  $16 \pm 3 \text{ kpc}$  at  $z = 0.10 \pm 0.02$ . Assuming random orientations this corresponds to a median physical separation  $r = 20 \pm 4 \text{ kpc}$ . To obtain an estimate of  $v_c$  we assume that the pairs have similar line-of-sight velocity differences as the seven elliptical-elliptical mergers discussed in Combes et al. (1995). The mean velocity difference of the Combes et al. pairs  $\Delta v = 296 \pm 91 \text{ km s}^{-1}$  (with the error determined by the jackknife method), implying  $v_c = \sqrt{3} \Delta v = 513 \pm 158 \text{ km s}^{-1}$  for an isotropic velocity distribution. The median mass of the companions is  $(7 \pm 3) \times 10^{10} M_\odot$ , where we used  $M/L_R = 4.6$  in Solar units to convert luminosity to mass (van der Marel 1991) and assumed  $z = 0.10 \pm 0.02$ . Taking  $\ln \Lambda \sim 2$  (following Dubinski et al. 1999 and Patton et al. 2000) we obtain  $T_{\text{fric}} = 0.4 \pm 0.2 \text{ Gyr}$ . With  $f_m = 19/122 = 0.16 \pm 0.03$  we obtain  $R = 0.4 \pm 0.2 \text{ Gyr}^{-1}$ .

The effect of the mergers on the mass evolution of red galaxies not only depends on the merger rate but also on the mass change resulting from individual mergers. The mass accretion rate can be approximated by

$$\Delta M/M = R \times \overline{M_2/M_1} \text{ Gyr}^{-1}, \quad (8)$$

with  $\overline{M_2/M_1}$  the median mass ratio of the mergers. As shown in § 6.2 this ratio is approximately 0.23. With  $R_m = 0.4$  we obtain  $\Delta M/M = 0.09 \pm 0.04 \text{ Gyr}^{-1}$ , i.e., merging increases the masses of galaxies on the red sequence by  $\sim 10\%$  every  $10^9$  years.

For comparison to other studies it is also of interest to consider the major merger fraction within a projected separation of 20 kpc. There are seven red pairs with luminosity ratio  $> 0.3$  and projected separation  $< 11''$ , corresponding to a fraction of  $0.06 \pm 0.02$ . It should be stressed that this number refers to mergers within the red sequence, not to the merger fraction within the full sample of  $R < 17$  galaxies. The colors of the well-separated pairs show that red galaxies “prefer” to merge with other red galaxies. We have not examined the prevalence of mergers among luminous blue galaxies, but as discussed in § 1 the stellar populations of ellipticals rule out widespread major mergers among this population. Therefore, the major merger rate in the full sample of red and blue galaxies is presumably much lower than that within the restricted sample of red galaxies. A very rough estimate of the merger fraction in the full sample is  $0.06 \times N_{\text{red}}/N_{\text{total}} \sim 0.02$ , in reasonable agreement with previous studies of close pairs (see, e.g., Patton et al. 2002, Lin et al. 2004, and references therein).

### 6.4. Effects on the Evolution of the Luminosity Density

At redshifts  $z < 1$ , the observed evolution of the luminosity function of red galaxies reflects passive evolution of the stellar populations and possible changes in the underlying mass function. As discussed in, e.g., McIntosh et al. (2005) these changes can be due to mergers, galaxies entering the red sample due to changes in their star formation rate, or other effects. The best available constraints on the evolution of the luminosity function of red galaxies were derived by Bell et al. (2004), using the COMBO-17 survey. They find that the luminosity density of luminous red galaxies is approximately constant out to  $z \sim 1$ , which is surprising given the expected evolution of a factor of 3–4 in the  $M/L$  ratios of the galaxies (e.g., van Dokkum et al. 1998a, Treu et al. 2005, van der Wel et al. 2005). A possible explanation is that the underlying stellar mass density evolves as well, compensating for passive evolution of the stellar populations (Bell et al. 2004).

We first determine the effect of the observed red mergers only, i.e., the 52 % of red galaxies that are merger remnants or a merger pair. Dry mergers have no effect on the total luminosity density, but they have a strong effect on the luminosity density of galaxies brighter than a fixed magnitude. The effect of a single generation of mergers can be approximated by

$$j(z) \approx \left(1 - f_m \left\langle \frac{L_2}{L_1 + L_2} \right\rangle\right) j(0), \quad (9)$$

with  $j(z)$  the luminosity density of luminous galaxies before the mergers and  $j(0)$  the luminosity density after the mergers. For  $f_m = 0.52$  and  $\langle L_2/L_1 \rangle = 0.3$  we find  $j(z) \approx 0.88j(0)$ . We use Monte Carlo simulations to test this approximation for a fiducial luminosity function with  $\alpha = -0.6$  and  $M_* = -19.9$  (Bell et al. 2004). The luminosity function is evolved backward in time by breaking 50 % of the galaxies into pieces with luminosity ratio 0.3. Calculating the luminosity density for  $M < -19$  gives  $j(z) = 0.89j(0)$ , in very good agreement with the simple estimate given above. The conclusion is that the effect of the observed mergers and remnants on the luminosity density of bright galaxies is small, of order 10 %.

The observed interactions only probe a relatively short period of at most a few Gyr. In order to extrapolate the effect of the mergers back in time we assume the following: 1) the mass accretion rate at  $z = 0.1$  is  $\Delta M/M = 0.09 \pm 0.04 \text{ Gyr}^{-1}$  (see § 6.3); 2) the change in luminosity density due to mergers is proportional to the accreted luminosity; 3) all red galaxies are equally likely to undergo mergers; and 4) the mass accretion rate evolves as  $(1+z)^m$ . The value of  $m$  is treated as a free parameter: observational constraints on the evolution of the merger rate may not be quite consistent (see, e.g., Patton et al. 2002, Concelice et al. 2003, Lin et al. 2004), and no studies have specifically considered the evolution of the pair fraction among galaxies on the red sequence.

The dashed lines in Fig. 10 show the predicted merger-driven evolution of the luminosity density of bright red galaxies with these assumptions, for three values of  $m$ . The model with  $m = 0$  has a constant accretion rate, and in the model with  $m = 1.5$  the accretion rate is  $3\times$  higher at  $z = 1$  than it is at

$z = 0$ . The dotted lines show the evolution of the  $M/L_B$  ratio of field early-type galaxies, as measured by van der Wel et al. (2005). These authors find  $\Delta \ln M/L_B = (-1.20 \pm 0.18)z$  for galaxies with  $M > 2 \times 10^{11} M_\odot$  (appropriate for our sample), which is consistent with the independent measurement by Treu et al. (2005). The solid line shows the predicted evolution of  $j_B$  when both mergers and  $M/L$  evolution are taken into account. Grey bands indicate the combined uncertainties in  $\Delta \ln M/L_B$  and the merger rate. The predicted evolution of  $j_B$  depends rather strongly on the assumed evolution of the mass accretion rate: it is positive for a non-evolving accretion rate, constant for  $m = 1$ , and negative for  $m > 1$ .

Solid points show the luminosity density in luminous red galaxies as measured by Bell et al. (2004) (their Fig. 5). As discussed extensively by these authors the data are inconsistent with passive evolution alone (dotted curves). However, as can be seen in Fig. 10 the data are fully consistent with models that include the mass accretion rate measured here. The uncertainties in the datapoints, the measured  $M/L$  evolution, and the merger rate are too large to distinguish between models with different values of  $m$ , although the data at  $z > 0.8$  seem to favor models with  $m > 0$ .

We infer that the cumulative effects of dry mergers may be the dominant cause of the constant luminosity density of luminous red sequence galaxies in the COMBO-17 survey. There are several caveats: both the datapoints in Fig. 10 and the  $z = 0.1$  mass accretion rate have substantial errors, leading to a wide range of allowed models; although the most recent generation of mergers appears to be (nearly) dissipationless, this may no longer hold at  $z \gtrsim 0.5$ ; and the fact that disk-dominated red galaxies probably evolve differently from bulge-dominated ones is ignored. The lack of evolution in the luminosity density of bright red galaxies, if confirmed, is probably due to a combination of effects with dry merging a significant, but not the only, contributor (see also McIntosh et al. 2005).

## 7. CONCLUSIONS

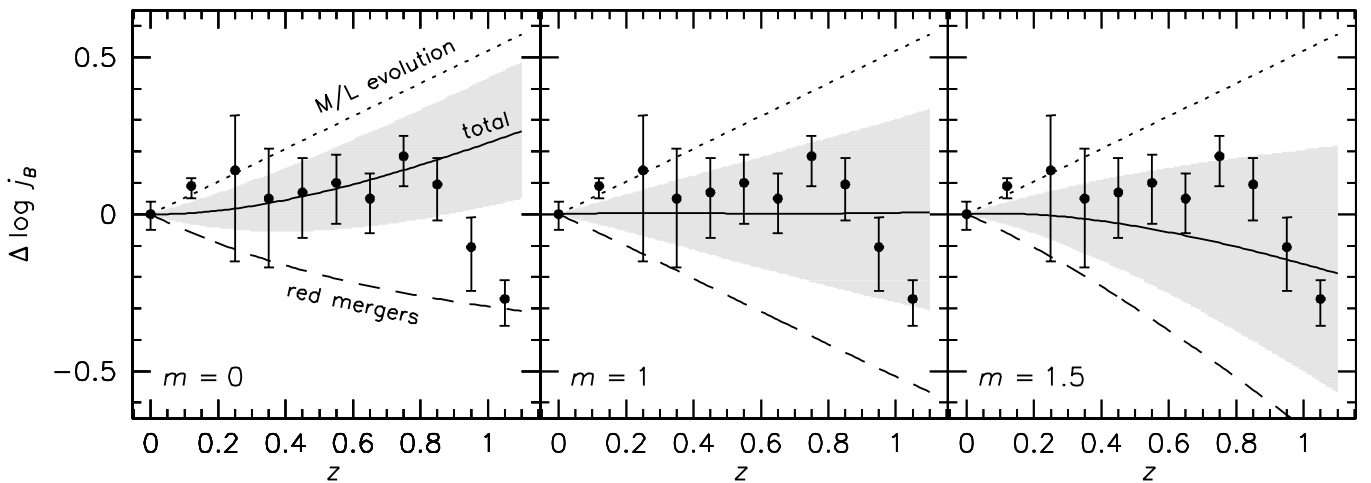


FIG. 10.— Evolution of the  $B$ -band luminosity density of red galaxies. The dotted lines show the evolution of the  $M/L_B$  ratio of field early-type galaxies, as measured by van der Wel et al. (2005). Dashed lines show the counter-acting effect of red mergers, with different assumptions for the evolution of the mass accretion rate. The mass accretion rate is  $9\% \pm 4\%$  per Gyr at  $z = 0.1$ , and evolves as  $(1+z)^m$ . The solid line shows the total luminosity density. Grey bands show the combined uncertainty resulting from the uncertainty in the merger rate and the evolution of the  $M/L_B$  ratio. Data points are from the Bell et al. (2004) analysis of the COMBO-17 dataset. There is good agreement between the models and the data, in particular if  $m > 0$ .

From an analysis of tidal features associated with bright red galaxies we find that  $\sim 70\%$  of bulge-dominated galaxies experienced a merger with median mass ratio 1:4 in the recent past. Expressed in other ways,  $\sim 35\%$  of bulge-dominated galaxies experienced a major merger involving  $> 20\%$  of its final mass, and the current mass accretion rate of galaxies on the red sequence  $\Delta M/M = 0.09 \pm 0.04 \text{ Gyr}^{-1}$ . Assuming a constant or increasing mass accretion rate with redshift it is inferred that the stellar mass density in luminous red galaxies has increased by a factor of  $\gtrsim 2$  over the redshift range  $0 < z < 1$ .

Neither of the two standard paradigms for elliptical galaxy formation appears to be consistent with our results: “monolithic” assembly at high redshift or late assembly via mergers of gas-rich disk galaxies. Instead, elliptical galaxies appear to have been assembled in mergers of bulge-dominated, red galaxies. This “dry” form of merging is qualitatively consistent with the high central densities of ellipticals (Gao et al. 2004), their red colors and uniform properties, the existence of the  $M_\bullet - \sigma$  relation (Wyithe & Loeb 2005), and their specific frequency of globular clusters.

It remains to be seen whether widespread dry mergers are consistent with the slope and scatter of the color-magnitude relation (see, e.g., Bower et al. 1998). The median merger in our sample makes the brightest galaxy more luminous by  $\sim 30\%$  and bluer by only  $\sim 0.02$  mag in  $B - R$ , and its remnant will lie within  $\sim 0.03$  mag of the color-magnitude relation. However, it is doubtful whether multiple generations of such mergers can be accommodated, unless there is a strong correlation between the masses of the progenitors (see Peebles 2002). It will also be interesting to see whether the evolution is consistent with the number density of massive galaxies at high redshift. Again, the *observed* mergers only have a  $\sim 10\%$  effect on the mass function of red galaxies, and the extrapolation to higher redshifts is obviously still very uncertain. Furthermore, the evolution of the mass function of all galaxies may be different from that of the subset of galaxies on the red sequence.

The high merger rate confirms predictions from hierarchical galaxy formation models in a  $\Lambda$ CDM universe (e.g., Kauffmann et al. 1993; Kauffmann 1996; Cole et al. 2000; Somerville, Primack, & Faber 2001; Murali et al. 2002). Furthermore, semi-analytical models have predicted that gas-poor mergers between bulge-dominated systems, rather than mergers of disk systems, are responsible for the formation of the most massive ellipticals (Kauffmann & Haehnelt 2000; and, in particular, Khochfar & Burkert 2003). Quantitative comparisons of mass growth are difficult as current models do not naturally produce red field galaxies without star formation: the colors of field ellipticals in the simulations are too blue and their  $M/L$  ratios too low (e.g., Kauffmann 1996; van Dokkum et al. 2001a). Additional mechanisms, such as heating by active nuclei, appear to be required to halt gas cooling and star formation in massive galaxies (e.g., Binney 2004, Somerville 2004, Dekel & Birnboim 2005, Keres et al. 2005). Our results imply that revised models which address these issues should not only reproduce the “red and dead” nature of ellipticals today but also of their immediate progenitors – which may occur naturally if the progenitors have masses greater than some critical mass (see Cooray & Milosavljević 2005).

The main uncertainty in the observed merger fraction is the possibility that the Northern NDWFS field, which contains over 90% of the sample, is special in its frequency of tidally disturbed objects. This seems unlikely given its area

of  $\sim 400 \text{ Mpc}^2$  at  $z = 0.1$ , but the issue of field-to-field variations in the merger fraction will only be settled conclusively when independent fields of similar size are studied in the same way. The main uncertainty in the merger *rate* and mass accretion rate is the timescale of the mergers. Although our estimates broadly agree with other studies (see, e.g., Lin et al. 2004, and references therein), this may simply reflect the fact that similar assumptions lead to similar results. Modeling of red, gas-poor mergers has not been done in a systematic way using modern techniques, and it will be interesting to see what the timescales are for the initial coalescence and the subsequent surface brightness evolution of tidal debris. Specifically, modeling of the 19 merging systems and 44 remnants presented here would provide much better constraints on the merger rate and mass accretion rate, particularly when more complete redshift information is available.

More detailed observational studies of the mergers and their remnants may help answer the question *why* the mergers are red, i.e., what made the progenitors lose their gas? If active nuclei prevent the cooling of gas above some critical mass at early times they may play the same role during mergers, and it will be interesting to compare the degree of nuclear activity in undisturbed galaxies, ongoing mergers, and remnants. Also, sensitive diagnostics of young populations (e.g., H $\delta$  line strengths and ultra-violet photometry) can provide better constraints on the star formation histories of the mergers and remnants. Finally, studies with higher spatial resolution can provide information on the detailed isophotal shapes (boxy or disk) of the remnants and their progenitors, and on possible correlations between large scale smooth distortions and the sharp ripples and shells that have been reported in  $z \approx 0$  ellipticals (see Hernquist & Spergel 1995).

Our study focuses on events that we can see today, and it will be very interesting to push the analysis to higher redshifts. Although the most recent generation of mergers could be largely “dry”, previous generations likely involved blue galaxies and/or were accompanied by strong star formation (see, e.g., Sanders et al. 1988). Unfortunately it will be difficult to identify the broad red tidal features that we see here at significantly higher redshift due to the  $(1+z)^4$  cosmological surface brightness dimming. The limiting depth of the MUSYC and NDWFS images is  $\sim 29 \text{ mag arcsec}^{-2}$  ( $1\sigma$ , AB). An equivalent survey at  $z \geq 1$  should cover an area of  $\gtrsim 1$  square degree and reach levels of  $\sim 31.5 \text{ mag arcsec}^{-2}$  at  $z = 1$  and  $\sim 33.5 \text{ mag arcsec}^{-2}$  at  $z = 2$ . Even when (unfavorable)  $K$ -corrections are ignored these requirements are well beyond the capabilities of current ground- or space-based telescopes. A more viable technique is to focus on the fraction of red galaxies in pairs. Although pair statistics require large corrections due to the short timescale of the mergers, pairs are easily detectable out to high redshift with the Hubble Space Telescope (see van Dokkum et al. 1999). Based on the work presented here the merger fraction among galaxies on the red sequence should be  $(0.06 \pm 0.02) \times (1+z)^m$  for separations  $< 20 \text{ kpc}$  and luminosity ratios  $\geq 0.3$ .

This paper was made possible by the dedicated efforts of all the individuals behind the NOAO Deep Wide-Field Survey and the Multi-wavelength Survey by Yale-Chile. Particular thanks go to Buell Januzzi and Arjun Dey for initiating and executing the NDWFS and to Eric Gawiser, who is the driving force behind MUSYC. David Herrera is responsible for reducing most of the MUSYC optical imaging data. Marijn Franx and Jeff

Kenney are thanked for useful discussions. Comments of the anonymous referee improved the paper significantly. The ND-WFS is supported by the National Optical Astronomy Obser-

vatory (NOAO). NOAO is operated by AURA, Inc., under a cooperative agreement with the National Science Foundation.

## REFERENCES

- Abraham, R. G., Tanvir, N. R., Santiago, B. X., Ellis, R. S., Glazebrook, K., & van den Bergh, S. 1996, *MNRAS*, 279, L47
- Arp, H. 1966, *ApJS*, 14, 1
- Balcells, M. & Quinn, P. J. 1990, *ApJ*, 361, 381
- Barnes, J. & Hut, P. 1986, *Nature*, 324, 446
- Becker, R. H., Fan, X., White, R. L., Strauss, M. A., Narayanan, V. K., Lupton, R. H., Gunn, J., et al. 2001, *AJ*, 122, 2850
- Bell, E. F., Wolf, C., Meisenheimer, K., Rix, H., Borch, A., Dye, S., Kleinheinrich, M., et al. 2004, *ApJ*, 608, 752
- Bender, R. 1988, *A&A*, 202, L5
- Bernardi, M., Renzini, A., da Costa, L. N., Wegner, G., Alonso, M. V., Pellegrini, P. S., Rit , C., & Willmer, C. N. A. 1998, *ApJ*, 508, L143
- Bernardi, M., Sheth, R. K., Annis, J., Burles, S., Finkbeiner, D. P., Lupton, R. H., Schlegel, D. J., et al. 2003, *AJ*, 125, 1882
- Bertin, E. & Arnouts, S. 1996, *A&AS*, 117, 393
- Binney, J. 2004, *MNRAS*, 347, 1093
- Binney, J., & Tremaine, S. 1987, *Galactic Dynamics* (Princeton: Princeton Univ. Press)
- Blanton, M. R., Dalcanton, J., Eisenstein, D., Loveday, J., Strauss, M. A., SubbaRao, M., Weinberg, D. H., et al. 2001, *AJ*, 121, 2358
- Bower, R. G., Kodama, T., & Terlevich, A. 1998, *MNRAS*, 299, 1193
- Bower, R. G., Lucey, J. R., & Ellis, R. S. 1992, *MNRAS*, 254, 601
- Boylan-Kolchin, M., Ma, C.-P., & Quataert, E. 2005, *MNRAS*, submitted (astro-ph/0502495)
- Carlberg, R. G. 1986, *ApJ*, 310, 593
- Colbert, J. W., Mulchaey, J. S., & Zabludoff, A. I. 2001, *AJ*, 121, 808
- Cole, S., Lacey, C. G., Baugh, C. M., & Frenk, C. S. 2000, *MNRAS*, 319, 168
- Coleman, G. D., Wu, C.-C., & Weedman, D. W. 1980, *ApJS*, 43, 393
- Combes, F., Rampazzo, R., Bonfanti, P. P., Pringniel, P., & Sulentic, J. W. 1995, *A&A*, 297, 37
- Conselice, C. J., Bershad, M. A., Dickinson, M., & Papovich, C. 2003, *AJ*, 126, 1183
- Cooray, A., & Milosavljevic, M. 2005, *ApJL*, submitted (astro-ph/0503596)
- Daddi, E., Cimatti, A., Renzini, A., Vernet, J., Conselice, C., Pozzetti, L., Mignoli, M., Tozzi, P., et al. 2004, *ApJ*, 600, L127
- Davoust, E., & Prugniel, P. 1988, *A&A*, 201, L30
- Dekel, A., & Birnboim, Y. 2005, preprint (astro-ph/0412300)
- Dey, A., et al. 2005, submitted
- Djorgovski, S. & Davis, M. 1987, *ApJ*, 313, 59
- Dubinski, J., Mihos, J. C., & Hernquist, L. 1996, *ApJ*, 462, 576
- Eggen, O. J., Lynden-Bell, D., & Sandage, A. R. 1962, *ApJ*, 136, 748
- Ellis, R. S., Smail, I., Dressler, A., Couch, W. J., Oemler, A. J., Butcher, H., & Sharples, R. M. 1997, *ApJ*, 483, 582
- Ferrarese, L. & Merritt, D. 2000, *ApJ*, 539, L9
- Franx, M., Illingworth, G., & Heckman, T. 1989, *AJ*, 98, 538
- Franx, M. & Illingworth, G. D. 1988, *ApJ*, 327, L55
- Franx, M., Labb , I., Rudnick, G., van Dokkum, P. G., Daddi, E., F rster Schreiber, N. M., Moorwood, A., Rix, H., et al. 2003, *ApJ*, 587, L79
- Fukugita, M., Shimasaku, K., Ichikawa, T. 1995, *PASP*, 107, 945
- Fukugita, M., Hogan, C. J., & Peebles, P. J. E. 1998, *ApJ*, 503, 518
- Gal, R. R., de Carvalho, R. R., Lopes, P. A. A., Djorgovski, S. G., Brunner, R. J., Mahabal, A., & Odewahn, S. C. 2003, *AJ*, 125, 2064
- Gao, L., Loeb, A., Peebles, P. J. E., White, S. D. M., Jenkins, A. 2004, *ApJ*, 614, 17
- Gawiser, E., et al. 2005, *ApJS*, submitted
- Gebhardt, K., Bender, R., Bower, G., Dressler, A., Faber, S. M., Filippenko, A. V., Green, R., Grillmair, C., et al. 2000, *ApJ*, 539, L13
- Glazebrook, K., Abraham, R. G., McCarthy, P. J., Savaglio, S., Chen, H., Crampton, D., Murowinski, R., J rgensen, I., et al. 2004, *Nature*, 430, 181
- Gonz lez-Garc a, A. C. & van Albada, T. S. 2003, *MNRAS*, 342, L36
- Hernquist, L. 1992, *ApJ*, 400, 460
- Hernquist, L., & Spergel, D. N. 1995, *ApJ*, 399, L117
- Hibbard, J. E. & van Gorkom, J. H. 1996, *AJ*, 111, 655
- Holden, B. P., van der Wel, A., Franx, M., Illingworth, G. D., Blakeslee, J. P., van Dokkum, P., Ford, et al. 2005, *ApJ*, 620, L83
- Hunsberger, S. D., Charlton, J. C., & Zaritsky, D. 1996, *ApJ*, 462, 50
- Ibata, R., Irwin, M., Lewis, G., Ferguson, A. M. N., & Tanvir, N. 2001, *Nature*, 412, 49
- Jansen, R. A., Franx, M., Fabricant, D., & Caldwell, N. 2000, *ApJS*, 126, 271
- Januzzi, B. T., & Dey, A. 1999, in "Photometric Redshifts and the Detection of High Redshift Galaxies", ASP Conference Series, Vol. 191, R. Weyman, L. Storrie-Lombardi, M. Sawicki, and R. Brummer, Eds., p. 111
- Januzzi, B. T., et al. 2005, submitted
- Jimenez, R., Friaca, A. C. S., Dunlop, J. S., Terlevich, R. J., Peacock, J. A., & Nolan, L. A. 1999, *MNRAS*, 305, L16
- Johnston, K. V., Sackett, P. D., & Bullock, J. S. 2001, *ApJ*, 557, 137
- J rgensen, I., Franx, M., & Kj rsgaard, P. 1995, *MNRAS*, 273, 1097
- J rgensen, I., Franx, M., & Kj rsgaard, P. 1996, *MNRAS*, 280, 167
- Kauffmann, G. 1996, *MNRAS*, 281, 487
- Kauffmann, G. & Haehnelt, M. 2000, *MNRAS*, 311, 576
- Kauffmann, G., White, S. D. M., & Guiderdoni, B. 1993, *MNRAS*, 264, 201
- Keres, D., Katz, N., Weinberg, D. H., Dave, R. 2005, *MNRAS*, submitted (astro-ph/0407095)
- Khochfar, S. & Burkert, A. 2003, *ApJ*, 597, L117
- Lin, L., et al. 2004, *ApJ*, 617, L9
- L pez-Cruz, O., Barkhouse, W. A., & Yee, H. K. C. 2004, *ApJ*, 614, 679
- Le F vre, O., Abraham, R., Lilly, S. J., Ellis, R. S., Brinchmann, J., Schade, D., Tresse, L., et al. 2000, *MNRAS*, 311, 565
- Makino, J. & Hut, P. 1997, *ApJ*, 481, 83
- Malin, D. F. & Carter, D. 1983, *ApJ*, 274, 534
- McIntosh, D. H., Bell, E. F., Rix, H.-W., Wolf, C., Heymans, C., Peng, C. Y., Somerville, R. S., Barden, M. 2005, *ApJ*, submitted (astro-ph/0411772)
- Meza, A., Navarro, J. F., Steinmetz, M., & Eke, V. R. 2003, *ApJ*, 590, 619
- Mihos, J. C. 1995, *ApJ*, 438, L75
- Mirabel, I. F., Dottori, H., & Lutz, D. 1992, *A&A*, 256, L19
- Murali, C., Katz, N., Hernquist, L., Weinberg, D. H., & Dav , R. 2002, *ApJ*, 571, 1
- Nakamura, O., Fukugita, M., Yasuda, N., Loveday, J., Brinkmann, J., Schneider, D. P., Shimasaku, K., & SubbaRao, M. 2003, *AJ*, 125, 1682
- Ostriker, J. P. 1980, *Comments on Astrophysics*, 8, 177
- Patton, D. R., Carlberg, R. G., Marzke, R. O., Pritchett, C. J., da Costa, L. N., & Pellegrini, P. S. 2000, *ApJ*, 536, 153
- Patton, D. R., Pritchett, C. J., Carlberg, R. G., Marzke, R. O., Yee, H. K. C., Hall, P. B., Lin, H., et al. 2002, *ApJ*, 565, 208
- Peebles, P. J. E. 2002, in "A new era in cosmology", ASP Conference Series, Vol. 283, N. Metcalfe and T. Shanks, Eds., p. 351
- Peletier, R. F., Davies, R. L., Illingworth, G. D., Davis, L. E., & Cawson, M. 1990, *AJ*, 100, 1091
- Pildis, R. A., Bregman, J. N., & Schombert, J. M. 1995, *AJ*, 110, 1498
- Rix, H. R. & White, S. D. M. 1989, *MNRAS*, 240, 941
- Sandage, A., & Visvanathan, N. 1978, *ApJ*, 223, 707
- Sanders, D. B., Soifer, B. T., Elias, J. H., Madore, B. F., Matthews, K., Neugebauer, G., & Scoville, N. Z. 1988, *ApJ*, 325, 74
- Sansom, A. E., Hibbard, J. E., & Schweizer, F. 2000, *AJ*, 120, 1946
- Schweizer, F. 1982, *ApJ*, 252, 455
- Schweizer, F., Miller, B. W., Whitmore, B. C., & Fall, S. M. 1996, *AJ*, 112, 1839
- Schweizer, F., Seitzer, P., Faber, S. M., Burstein, D., Dalle Ore, C. M., Gonz lez, J. J. 1990, *ApJ*, 364, L33
- Schweizer, F. & Seitzer, P. 1992, *AJ*, 104, 1039
- Somerville, R. S. 2004, in "Coevolution of Black Holes and Galaxies", L. C. Ho, Ed., Cambridge University Press, p. 391
- Somerville, R. S., Primack, J. R., & Faber, S. M. 2001, *MNRAS*, 320, 504
- Spergel, D. N., et al. 2003, *ApJS*, 148, 175
- Stratava, I., et al. 2001, *AJ*, 122, 1861
- Tonry, J. L., Howell, S. B., Everett, M. E., Rodney, S. A., Willman, M., & VanOortyve, C. 2005, *PASP*, 117, 281
- Toomre, A. & Toomre, J. 1972, *ApJ*, 178, 623
- Trager, S. C., Faber, S. M., Worthey, G., & Gonz lez, J. J. 2000, *AJ*, 119, 1645
- Tran, K.-V., van Dokkum, P. G., Franx, M., Illingworth, G. D., Kelson, D. D., F rster Schreiber, N. 2005, *ApJ*, 627, L25
- Treu, T., Stiavelli, M., Casertano, S., Moller, P., & Bertin, G. 1999, *MNRAS*, 308, 1037
- , 2002, *ApJ*, 564, L13
- Treu, T., Ellis, R. S., Liao, T. X., & van Dokkum, P. G. 2005, *ApJ*, 622, L5
- van der Marel, R. P. 1991, *MNRAS*, 253, 710
- van der Wel, A., Franx, M., van Dokkum, P. G., Rix, H.-W., Illingworth, G. D., & Rosati, P. 2005, *ApJ*, in press (astro-ph/0502228)
- van Dokkum, P. G. & Franx, M. 1995, *AJ*, 110, 2027
- , 2001, *ApJ*, 553, 90
- van Dokkum, P. G., Franx, M., Fabricant, D., Kelson, D. D., & Illingworth, G. D. 1999, *ApJ*, 520, L95
- van Dokkum, P. G., Franx, M., Kelson, D. D., & Illingworth, G. D. 1998a, *ApJ*, 504, L17
- , 2001a, *ApJ*, 553, L39
- van Dokkum, P. G., Franx, M., Kelson, D. D., Illingworth, G. D., Fisher, D., & Fabricant, D. 1998b, *ApJ*, 500, 714
- van Dokkum, P. G., Stanford, S. A., Holden, B. P., Eisenhardt, P. R., Dickinson, M., & Elston, R. 2001b, *ApJ*, 552, L101
- White, S. D. M. & Frenk, C. S. 1991, *ApJ*, 379, 52
- Wyithe, J. S. B., & Loeb, A. 2005, *ApJ*, submitted (astro-ph/0506294)
- Wolf, C., et al. 2005, *A&A*, submitted
- Yi, S. K., Yoon, S.-J., Kaviraj, S., Deharveng, J.-M., Rich, R. M., Salim, S., Boselli, A., et al. 2005, *ApJ*, 619, L111
- York, D. G., Adelman, J., Anderson, J. E., Anderson, S. F., Annis, J., Bahcall, N. A., Bakken, J. A., et al. 2000, *AJ*, 120, 1579



Zabludoff, A. I. & Mulchaey, J. S. 1998, ApJ, 496, 39  
Zepf, S. E., Whitmore, B. C., & Levison, H. F. 1991, ApJ, 383, 524

## APPENDIX

### CATALOG AND ATLAS

Here we provide coordinates, magnitudes, colors, morphologies, and tidal classifications for all 126 red galaxies. We also present images of all objects in the sample. These small images at fixed contrast level do not do the data justice, but space limitations prohibit an atlas on the scale of Figs. 3 and 4.

The atlas is available at [www.astro.yale.edu/dokkum/mergers/](http://www.astro.yale.edu/dokkum/mergers/) along with a version of the paper with **much** higher quality figures. The catalog will be made available on the same website after the paper is accepted for publication.

This figure "f1.jpg" is available in "jpg" format from:

<http://arxiv.org/ps/astro-ph/0506661v1>

This figure "f3.jpg" is available in "jpg" format from:

<http://arxiv.org/ps/astro-ph/0506661v1>

This figure "f4.jpg" is available in "jpg" format from:

<http://arxiv.org/ps/astro-ph/0506661v1>

This figure "f5.jpg" is available in "jpg" format from:

<http://arxiv.org/ps/astro-ph/0506661v1>

This figure "f7.jpg" is available in "jpg" format from:

<http://arxiv.org/ps/astro-ph/0506661v1>

This figure "f9.jpg" is available in "jpg" format from:

<http://arxiv.org/ps/astro-ph/0506661v1>